www.czasopisma.pan.pl PAN www.journals.pan.pl

Opto-Electronics Review 27 (2019) 282–290

Contents lists available at ScienceDirect

Opto-Electronics Review

journal homepage: http://www.journals.elsevier.com/opto-electronics review

MBE-grown MCT hetero- and nanostructures for IR and THz detectors

S.A. Dvoretsky[a,c], N.N. Mikhailov[a,d,*], V.G. Remesnik[a], Yu.G. Sidorov[a], V.A. Shvets[a], D.G. Ikusov[a], V.S. Varavin[a], M.V. Yakushev[a], J.V. Gumenjuk-Sichevska[b], A.G. Golenkov[b], I.O. Lysiuk[b], Z.F. Tsybrii[b], A.V. Shevchik-Shekera[b], F.F. Sizov[b], A.V. Latyshev[a], A.L. Aseev[a]

[a] *Rzanov Institute of Semiconductor Physics SB RAS, 13 Lavrentyev aven., Novosibirsk, 630090, Russia*
[b] *Lashkaryov Institute of Semiconductor Physics NAS, Ukraine, 41 Nauki aven., 03028, Kyiv, Ukraine*
[c] *Tomsk State University, 36 Lenin aven., 634050, Tomsk, Russia*
[d] *Novosibirsk State University, 1 Pirogov str., Novosibirsk, 630090, Russia*

ARTICLE INFO

Article history:
Received 13 December 2018
Received in revised form 17 July 2019
Accepted 18 July 2019
Available online 18 September 2019

Keywords:
Growth
HgCdTe
Molecular-beam epitaxy
Detector
Infrared
Terahertz

ABSTRACT

We present an overview of our technological achievements in the implementation of detector structures based on mercury cadmium telluride (MCT) heterostructures and nanostructures for IR and THz spectral ranges. We use a special MBE design set for the epitaxial layer growth on (013) GaAs substrates with ZnTe and CdTe buffer layers up to 3" in diameter with the precise ellipsometric monitoring *in situ*. The growth of MCT alloy heterostructures with the optimal composition distribution throughout the thickness allows for the realization of different types of many-layered heterostructures and quantum wells to prepare the material for fabricating single- or dual-band IR and THz detectors.

We also present the two-color broad-band bolometric detectors based on the epitaxial MCT layers that are sensitive in 150–300-GHz subterahertz and infrared ranges from 3 to 10 μm, which operate at the ambient or liquid nitrogen temperatures as photoconductors, as well as the detectors based on planar HgTe quantum wells. The design and dimensions of THz detector antennas are optimized for reasonable detector sensitivity values. A special diffraction limited optical system for the detector testing was designed and manufactured. We represent here the THz images of objects hidden behind a plasterboard or foam plastic packaging, obtained at the radiation frequencies of 70, 140, and 275 GHz, respectively.

1. Introduction

Today, the technical vision system based on the infrared (IR) detection is intensively used in human life for a wide range of applications. The wavelength dependence, in which the radiation flux of the energy for the black body with temperature T reaches its maximum (λmax), given by Wien displacement law, is expressed by equation λmax = 3000/T. It is clear that the wavelength in the range of 1–2.5 μm is typical of the temperatures of many terrestrial media. Three spectral ranges 1–3, 3–5 and 8–14 μm, the so-called "atmospheric windows", are most important because the IR radiation penetrates throughout the atmosphere practically without absorption. That allows detecting the temperature bodies at extended distances. To implement this, it is necessary to create a high-sensitivity imaging system based on a photosensitive material with high radiation absorption and high quantum efficiency. It is seen that the tunable bandgap HgCdTe (mercury cadmium telluride, MCT) compound covers the entire spectral range of "atmospheric windows" and has unique physical properties [1–3]. Nevertheless, it is also possible to realize the sensitivity in the terahertz (THz) spectral ranges [4,5].

The THz radiation (now 0.1–10 THz) is widely used in different areas of human activity, *i.e.* astronomy, THz imaging, security, biology, drugs and explosive material detection, *etc.* [6]. In spite of the significant efforts in scientific research activities and many papers [7,8], books and reviews [please, see Ref. 9], the THz applications, in general, are still at the early stage of their development. The interest in the THz frequency range is aroused by the fact that this range is the place, where different physical phenomena are revealed, and it frequently necessitates the special multidisciplinary knowledge in this research area. Therefore, the THz wave instrument capabilities are still far behind in comparison, *e.g.*, with the IR system feasibilities. In this work, we are focused at applying narrow-gap HgCdTe semiconductors and theirs quantum well structures in the development of uncooled direct THz detectors.

* Corresponding author at: Rzanov Institute of Semiconductor Physics SB RAS, 13 Lavrentyev aven., Novosibirsk, 630090, Russia.
E-mail address: mikhailov@isp.nsc.ru (N.N. Mikhailov).

https://doi.org/10.1016/j.opelre.2019.07.002
1230-3402/

The HgCdTe nanostructures are used as a promising material for developing a new generation of detectors, spintronic devices and studies of new physical phenomena [10–12]. It is necessary to point out that the small difference in lattice parameters at changing the HgCdTe composition allows for the development of multispectral detectors based on HgCdTe structures [5,13]. The HgCdTe technology was developed from the first paper about preparing a mixed CdTe-HgTe compound, fabricating bars of small volumes (diameter <10 mm) to the hetero-epitaxial layer grown by LPE, MOCVD or MBE methods on CdZnTe, GaAs and Si substrates (up to 6" in diameter) over the past almost 60 years [14,15]. The MBE technology has the following apparent advantages over other epitaxial methods:

- low growth temperatures of about 180 °C, in comparison with 450 °C for LPE and 300–400 °C for MOCVD, that effectively reduce the diffusion from the substrate and background doping, as well as sharpened interfaces between layers with different compositions,
- absence of an aggressive environment that, combined with low temperatures, allows using the so-called "alternative" GaAs substrates and Si substrates with CdTe and ZnTe buffer layers. HgCdTe heterostructures on a Si substrate give the material for developing cooled megapixel detectors because of the thermal expansion coefficient close to silicon readout circuits;
- possibility of carrying out the *in situ* growth control of HgCdTe heterostructures by the different analytical optoelectronic equipment that gives us the possibility of fabricating a planned design composition distribution over the thickness, especially for multicolor detectors;
- ideal technique for growing CdTe/HgTe superlattices and other nanostructures.

Here we present the review of our results for different MCT hetero- and nanostructures grown for IR and THz detections.

2. MCT heterostructures' growth

HgCdTe heterostructures were grown by the "Ob-M"- type MBE setup at ultra-high vacuum operating in the mercury atmosphere [16]. In Fig. 1, from left to right, are: the load-lock chamber, three technological chambers equipped by RHEED (reflection high-energy electron diffraction) and ultrafast single-wave ellipsometers and an unload-lock chamber. We use the ultrafast

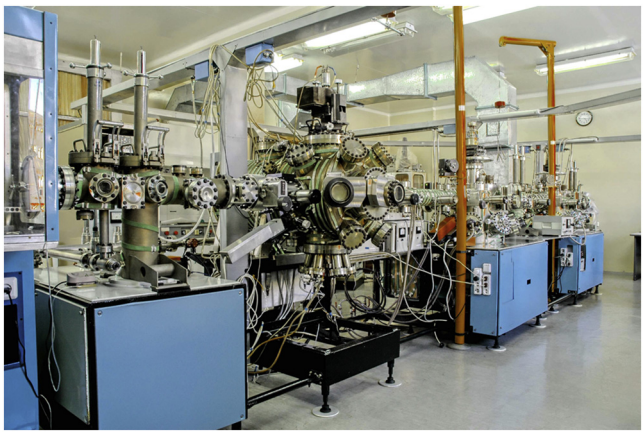

Fig. 1. Photo MBE setup "Ob-M" type.

single-wave ellipsometer to monitor the growth process in the technological chambers in real time [17,18]. The scheme of built-in ultrafast single-wave ellipsometer is shown in Fig. 2. We can reach a high-precision measurement of the HgCdTe composition and thickness at measuring ellipsometric angles ψ and Δ with the accuracy of 0.01° (see specifications in Fig. 2). To control the composition, we use the experimental dependence of the HgCdTe optical constants at incidence laser beam angle $\varphi = 70^0$ on the composition (mole fraction of CdTe in HgCdTe alloy X_{CdTe}) [19,20].

To control the thickness, we use the variation of ellipsometric parameters ψ and Δ in the ψ-Δ plane at the initial growth stage. The variation of ψ and Δ at the initial growth stage of HgCdTe layer with mole fraction $X_{CdTe} = 0.4$ on the CdTe/ZnTe/GaAs substrate [21] is demonstrated in Fig. 3. We see the variation of ellipsometric parameters at the initial stage represented as a convergent spiral. One can calculate the growth rate by measuring the time when the curve in Fig. 3 reaches the point that corresponds to a definite thickness value (numbers near the convergent curve). Therefore, we can determine the change of growth rate at the initial growth stage, stationary condition and the thickness by measuring the time during the sequence growth.

The scheme of layers in the most popular developed HgCdTe heterostructures grown by MBE on (013) GaAs or (013) Si substrates is shown in Fig. 4.

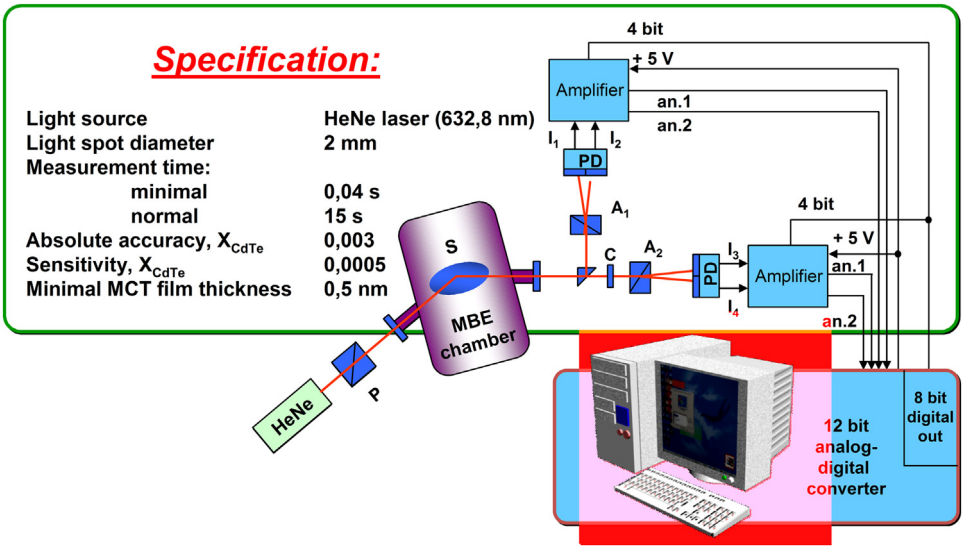

Fig. 2. The scheme of ultra fastsingle wave ellipsometer with a specification.

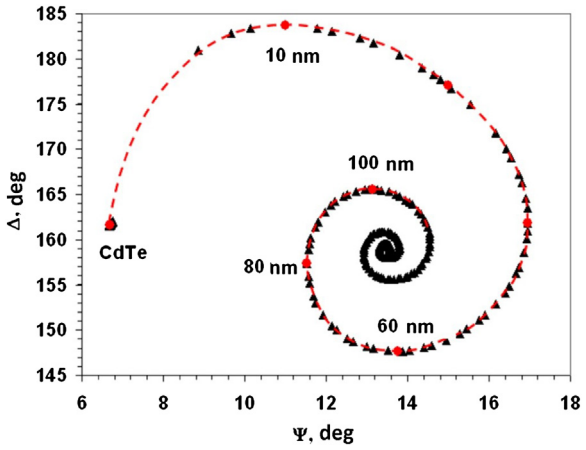

Fig. 3. The alternation of the ellipsometric parameters ψ and Δ during growth of HgCdTe film on CdTe/ZnTe/GaAs substrate at initial stage. Red dashed line shows the calculated curve. The numbers near the red circles indicate HgCdTe layer thickness. Triangles represent the experimental data.

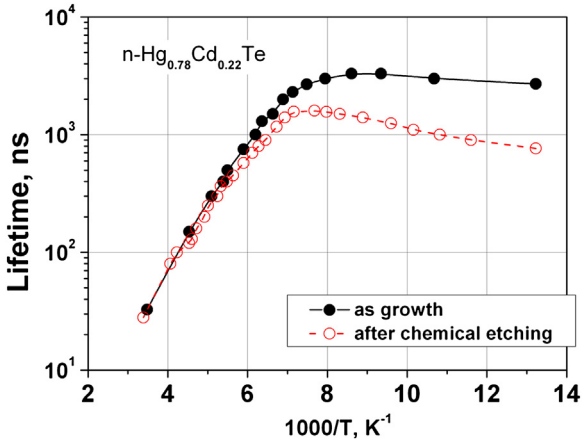

Fig. 6. The temperature dependence of the minority carrier lifetime (n - type material) of the HgCdTe absorber (XCdTe = 0,215) with the variable layer composition at the interface and towards the surface (curve 1), and without the variable layer composition towards the surface (curve 2) after the removing by chemical etching.

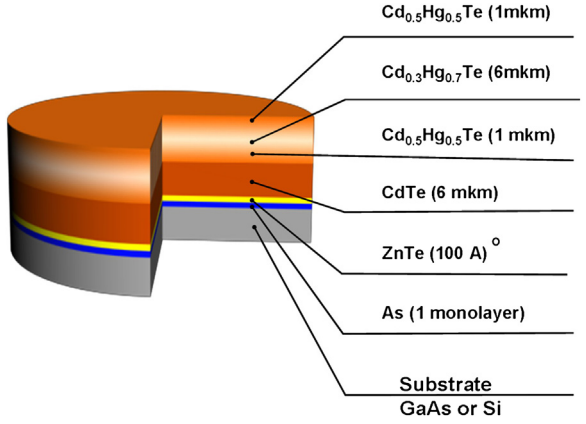

Fig. 4. The scheme of the typical HgCdTe heterostructure.

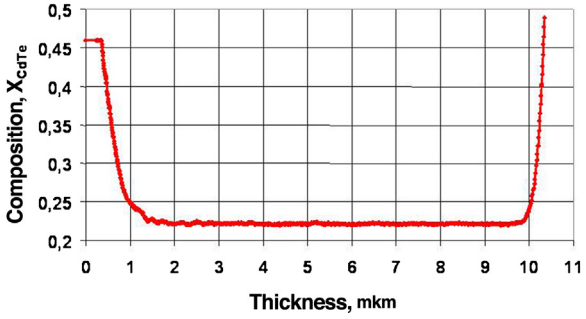

Fig. 5. HgCdTe composition distribution on the thickness of MBE film measured by *in-situ* ellipsometer.

The HgCdTe heterostructure growth begins from the thermal cleaning of (013) GaAs substrate surface. Then we grow the buffer layers ZnTe (0,01 μm) and CdTe (5–7 μm) to conserve the orientation and to eliminate the large lattice mismatch between HgCdTe and GaAs (13,6%). Then follows the HgCdTe absorber layer (in the scheme $X_{CdTe} = 0.3$), in which the composition was changed from $X_{CdTe} = 0.5$ up to $X_{CdTe} = 0.3$ at the interface and back from $X_{CdTe} = 0.3$ up to $X_{CdTe} = 0.5$ at the surface. In Fig. 5 is the HgCdTe composition change with the thickness for the heterostucture with a variable layer composition at the interface and towards the surface [22]. The variable gradient layers create the electric field that prevents the charge-carrier recombination, at the interface and on the surface, and surface leakage current [23].

In Fig. 6 is the temperature dependence of the minority carrier lifetime of the HgCdTe absorber ($X_{CdTe} = 0,22$) with the variable layer composition at the interface and towards the surface (curve 1), and without the variable layer composition towards the surface (curve 2) after the removing by chemical etching. That data were obtained from the nonequilibrium carrier relaxation excited by the SHF radiation.

The minority carrier lifetime at the temperature of 77 K is reduced 4–5 times, indicating the positive effect of variated-gap layers. It should be noted that the carriers concentration in the MCT structures with graded-gap layers does not differ from the one of the structures without variated-gap layers. Perhaps, dislocations do not affect the lifetime so much, as considered in [24].

The as-grown HgCdTe heterostructures are of n-type conductivity. The as-grown HgCdTe heterostructures are of n-type conductivity. For the n–p junction formation, it is necessary to obtain the p-type conductivity for applying the well-developed technology of p-type HgCdTe layers doped with Hg vacancies. For this purpose, the HgCdTe layer n-type conductivity converts to that of p-type by thermal annealing [25].

The hole concentration dependence on temperature for the MBE-grown HgCdTe layer (absorbers composition $X_{CdTe} = 0.21–0.23$ and $X_{CdTe} = 0.29–0.31$) and by LPE ($X_{CdTe} = 0.22$) at 77 K is presented in Fig. 7. This dataset was measured after the thermal annealing at the inert atmosphere during 24 h. The thermal annealing at 200–250 °C allows obtaining the hole concentration values of $10^{15}–10^{16}$ cm^{-3} that are optimal for good n–p junction parameters. The hole concentration of MBE and LPE HgCdTe with the layer composition $X_{CdTe} = 0.22$ after the thermal annealing are in a good agreement with each other. Therefore, we can conclude that the hole concentrations of the layers prepared by different epitaxial methods after the thermal annealing determine the same defects created by Hg vacancies.

For extending the range of electron concentration in the HgCdTe absorber layer, we study the intentional doping by indium (In). In Fig. 8 is the electron concentration (n) dependence on the In concentration in the HgCdTe bulk measured by SIMS (Secondary Ion Mass Spectrometry). The linear electron concentration dependence on the In concentration in Fig. 8 is the evidence of practically the 100% ionization of In atom on the metallic site of crystalline lattice. The minority lifetime is limited by Auger process at n values greater than 3×10^{15} cm^{-3} and the Shockley-Hall-Read (SHR)

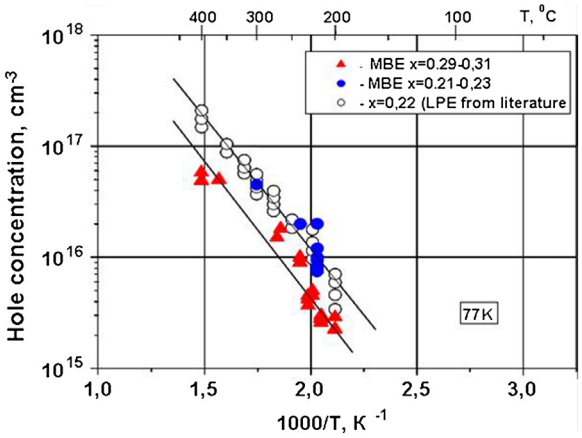

Fig. 7. The dependence of hole concentration on thermal annealing temperatures: ▲ -MBE HgCdTe (X_{CdTe} = 0.29–0.31); ● -MBE HgCdTe (X_{CdTe} = 0.21–0.23); ○-LPE HgCdTe (X_{CdTe} = 0.22).

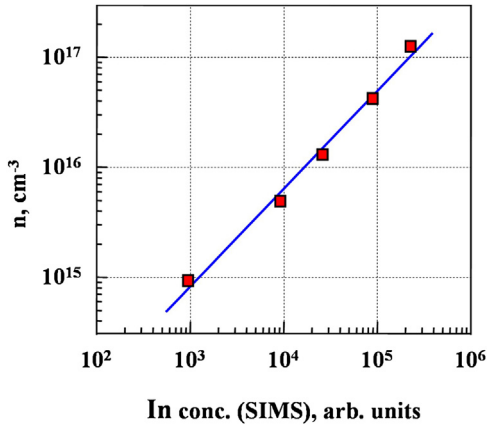

Fig. 8. The electron concentration dependence on In-impurity concentration: squares are the experimental points; the solid line is the linear approximation.

recombination at n values below 3×10^{15} cm^{-3}. The electron mobility is limited by scattering on ionized impurities and by optical phonons. The difference between the experimental and model data is connected with an additional scattering on inhomogeneity, neutral impurities or it is determined by their compensation. The indium doping allows growing HgCdTe with an electron concentration up to 10^{17} cm^{-3}. This enables us to create the HgCdTe composition distributions over the thickness for the high conductivity multielement (up to megapixels) IR detectors based on the p-type absorber.

The scheme of layer sequence in the HgCdTe nanostructure with the HgTe quantum well (QW) grown by MBE on (013) GaAs substrates is shown in Fig. 9. The single HgTe QW consists of the HgTe layer between wide-gap HgCdTe spacers doped by In (symmetrically or not) or undoped in the central parts. The multiple HgTe QW represents periodic single HgTe QW structures [26].

The evolution of ellipsometric parameters ψ and Δ during the single HgTe QW growth is shown in Fig. 10 as a sectional smooth curve in the ψ-Δ plane. Each smooth section corresponds to the constant MCT composition layers. Its length is determined by every layer thickness. The initial point O corresponds to the ellipsometric parameters of CdTe surface. The QW fabrication begins from the first spacer layer (x ~ 0.7) growth (curve O-A) after opening the tellurium and cadmium source shutters. Doping the central part of this layer is carried out by the indium doping process between the open-

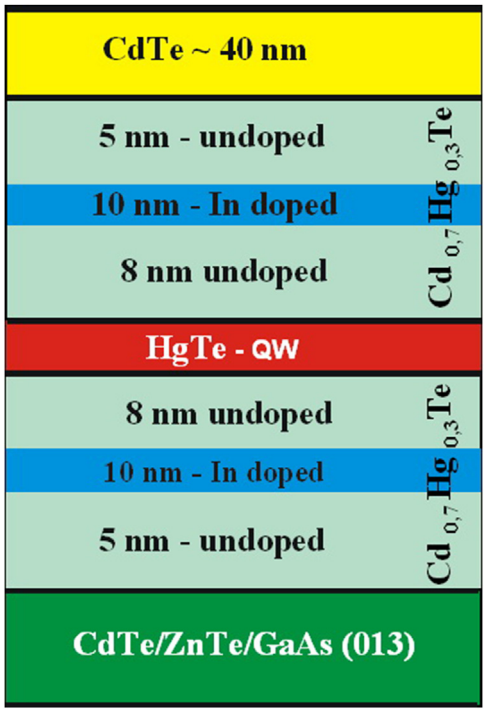

Fig. 9. The scheme of layers in the single HgTe QW structure.

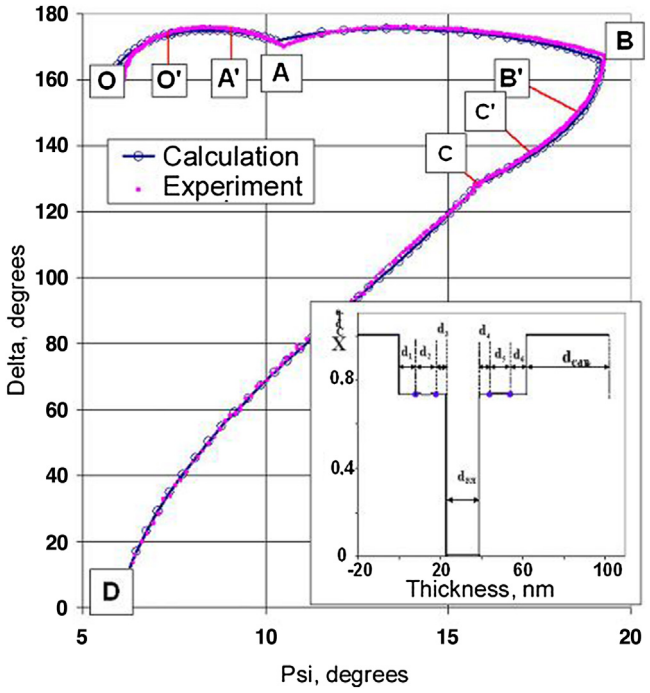

Fig. 10. The evolution of ellipsometric parameters D and y during the growth of HgTe QW. The points at the curve knees (O – C) correspond to initial stage of growth of following QW layer. Dots – experimental data; solid line and circles (through 1 nm) – calculated data. In the inset, the variation of MCT composition *versus* thickness is shown.

ings in O′ and closing in the A′ of indium source shutter. Then the wide-gap layer growth continues up to point A. In the insert, sectors O-O′, O′-A′ and A′-A correspond to the gradual spacer growth of the undoped layer with thickness d_1, In-doped layer with thickness d_2 and the undoped wide-gap layer with thickness d_3. After

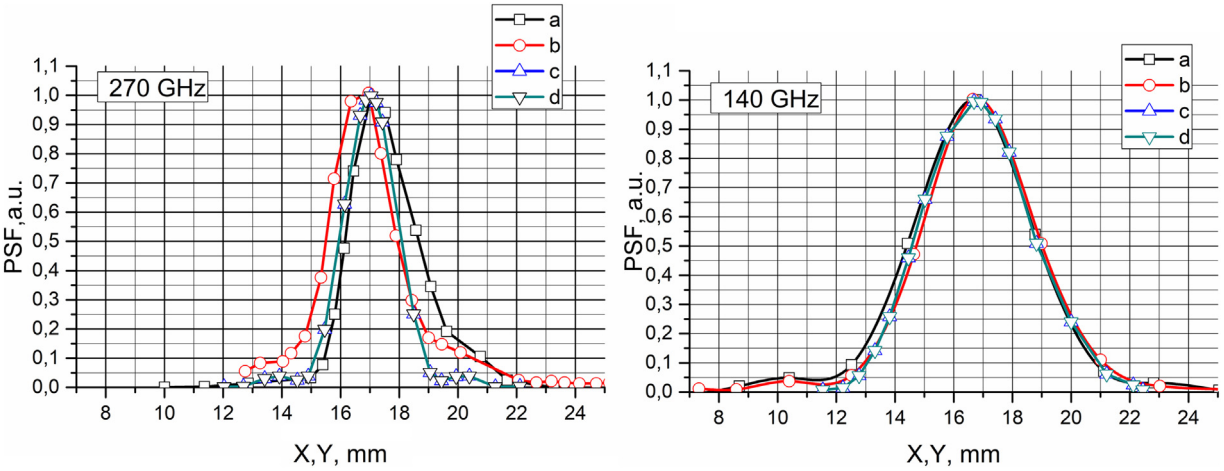

Fig. 11. The comparison of the experimental results (*a*, *b*) and computer modeling (*c*, *d*) of the point spread function fit through the maximum in *x* and *y*-direction for the system from two axially symmetric lenses with the aspherical surfaces with the focal length of 125 mm and the diameter of 80 mm.

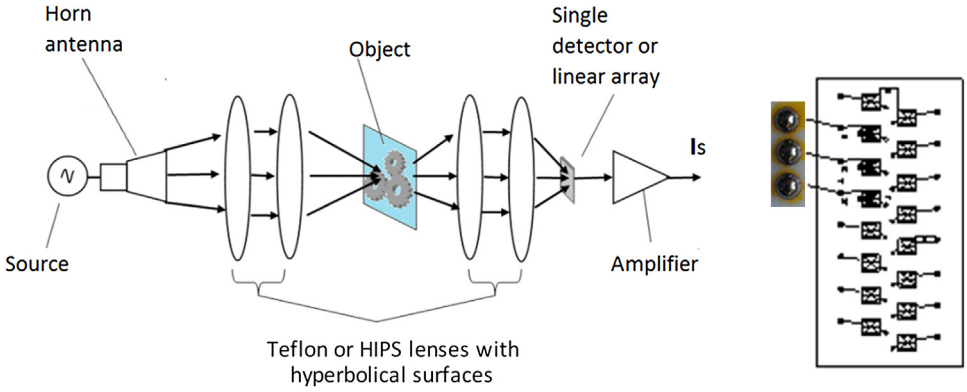

Fig. 12. The optical scheme, Si microlenses and 16-element MCT array used for obtaining the THz images.

closing the cadmium source shutter, the HgTe layer with thickness d_{QW} growths between the A–B points of ellipsometric curve. The second spacer layer (see B–C curve) growth is in the manner that is analogous to the first spacer layer (O-A curve) growth after opening the cadmium source shutter. Thicknesses d_4, d_6 and d_5 correspond to the undoped and In-doped parts of the second spacer layer, respectively. After all, the CdTe cap layer with $d_{CdTe} \sim 40$ nm covers the grown QW structure. The dots on the curve in Fig. 10 are the experimental data measured in the one-second interval. The circles correspond to the calculated values of the ellipsometric parameters at the 1 nm change of layer thickness. The calculations were carried out within the one-layer model [21]. The calibration curve and optical constants for the calculations were taken into account for different MCT compositions from [17,20]. It is necessary to know the optical constants of the substrate and growing layers with high accuracy at the incident light wavelength, and the growth temperature to improve the comparison of the experimental data with the calculated ones. The optical constants of different MCT compositions were obtained from the spectral measurements at room or lower temperatures [27,28]. These data cannot be used for calculating the ellipsometric parameter variations during the QW growth, which is carried out at much higher temperature values. Thus, we used the dependences of MCT composition optical constants (n(x) and k(x)), that were measured at room temperature [21], and then calculated the growth temperature using the experimentally determined thermo-optical coefficients. The experimental data are in a good agreement with the calculations (Fig. 10) in this procedure.

3. Development of THz quasi-optical system

To proceed with the experiments in the THz/sub-THz sensitivity and imaging, special optics should be developed. In the earlier papers [29,30], the THz quasi-optical system based on refractive aspherical lenses was proposed. Later, plastic PTFE (Polytetrafluoroethylene) of ultra-high molecular weight and the refractive index of 1.43 were selected as the lens material. The lenses were processed using a mechanical/polishing lathe, and it resulted in a surface roughness less than 30 μm (~λ/10). Here, for manufacturing the lenses, we used another approach related to the 3D printing capabilities, and it reduces the manufacturing time, increases the cost-efficiency and allows establishing a full cycle of creating aspherical THz lenses in one workplace. Both axially symmetrical and cylindrical lenses, calculated with the Zemax program, were manufactured using the 3D printing for applications requiring a single element and one-dimensional shaping of a light source, such as a linear array. In Fig. 11 are shown the XY cross-sections (at *z* – the focal plane of aspherical lenses) of the lenses with the focal length of $f = 125$ mm and the diameter, $a = 80$ mm, designed for the radiation frequencies $\nu = 270$ and 140 GHz. The lenses, which were designed were manufactured from the High Impact Polystyrene (HIPS).

In Fig. 11 is shown the comparison the comparison of the computer modeling (*c*, *d*) and the experimental results (*a*, *b*).

We designed and manufactured the active THz-imaging system consisting of the source combined with the horn emitter, lens system, scanning mirror, linear detecting array and an electronic

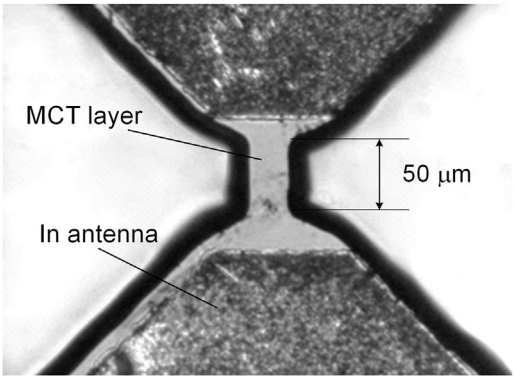

Fig. 13. MCT sensitive element with bow-tie antenna used both as THz and IR detector.

board with circuits for detector biasing, output signal multiplexing and amplification. The optical scheme used for obtaining the THz images is presented in Fig. 12. The first pair of lens focuses the radiation onto the object; the second focuses it onto the THz detector. The shown focusing properties are as expected and demonstrate the spot sizes that are close to the diffraction limit for the system with two axially symmetrical lenses.

4. MCT heterostructures THz/sub-THz sensitivity

The possibility of using the narrow-gap HgCdTe structures as uncooled or slightly cooled THz/sub-THz bolometer detectors was considered in Ref. [31]. The hot electron effect began to be applied in radiation detectors long ago [32].

In the model considerations [31], an electromagnetic wave from an antenna enters a bipolar semiconductor layer, propagates there as in a waveguide and heats the electrons and holes. Mainly, the free electrons in a $Hg_{1-x}Cd_xTe$ bolometer (the intrinsic concentration $n_i \sim 2{\cdot}10^{16}$ cm^{-3} at $x \sim 0.22$ and at $T \sim 300$ K) are heated by the electromagnetic wave field changing the bolometer resistance. Three types of hot electron effects are responsible for the MCT bolometer response: photo-diffusion effect, thermo-electromotive effect and the free carrier concentration changes.

In the bipolar narrow-gap HgCdTe epitaxial sensitive elements, the radiation frequency range being $\nu \sim 0.37$–1.54 THz, the observed temperature response can be satisfactorily described within the developed model (up to changing the sign of response) [33]. The observed radiation frequency ν dependence of the noise equivalent power (NEP) follows the dependence NEP $\sim \nu^{-2}$ considered in Ref. [34] for THz detectors with antennas.

In Ref. [35] the issues associated with the development of bi-color IR and THz direct detectors on the base of HgCdTe are discussed. Bi-color uncooled and cooled to 78 K narrow-gap mercury-cadmium-telluride (MCT) semiconductor thin layers ($d \sim 6$–8 μm) with antennas (see Fig. 13) were considered both as THz ($\nu \approx 128$–144 GHz radiation frequency range) direct detection bolometers and 3 to 10 μm infrared (IR) photoconductors. Sensitive layer thicknesses (~5 μm) were optimized for IR and sub-THz responses. The design of THz detector antennas, taking into account the thick dielectric substrate effects, is optimized for the reasonable detector sensitivity within the 150–300-GHz frequency range. Here we choose the simple bow-tie antenna configuration at the 90^0 divergence angle of the antenna side from the centre of the sensitive element. Such a simple detector construction allows using the antenna blades as symmetrical current contacts for a photocurrent registration in the IR spectral region.

The NEP for one of the detectors studied at $\nu \approx 140$ GHz reaches $NEP_{300K} \approx 4.5{\cdot}10^{-10}$ W/Hz$^{1/2}$ and $NEP_{78K} \approx 5{\cdot}10^{-9}$ W/Hz$^{1/2}$.

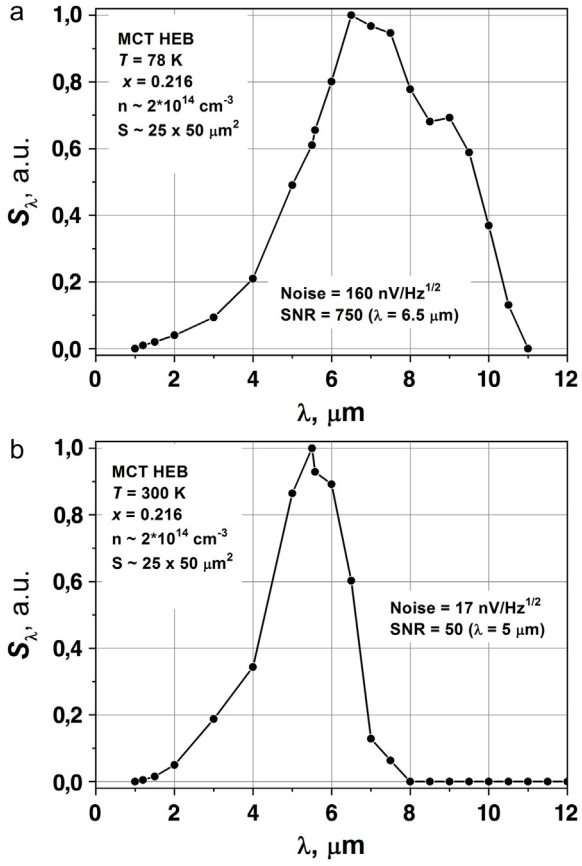

Fig. 14. Responsivity spectra of MCT photoconductor in the IR region: (a) T = 78 K, (b) T = 300 K. FOV = 180^0.

The same detector used as an IR photoconductor (Fig. 14) showed the responsivity at T = 78 K and 300 K with signal-to-noise ratios S/N ≈ 750 and 50. For the NEP estimations, the antennas effective area was used: $A_{eff} = (\lambda^2/4\pi){\cdot}G$, [36], where λ is the radiation wavelength, and the antenna directivity was taken as G = 1.

The basis for the IR response in a narrow-gap MCT, even at T = 300 K, is that the band-to-band optical absorption is a strong direct-gap MCT semiconductor. At $\lambda \approx 5$ μm and at T = 300 K, the absorption coefficient α in such layers is $\alpha \approx 5{\cdot}10^3$ cm^{-3}. Thus, in the active layers of thicknesses $d \approx 5$ μm, there is the strong absorption approximation ($\alpha{\cdot}d > 1$). Because of the diffusion length in the intrinsic $Hg_{1-x}Cd_xTe$ layers is much larger than the active layer thickness, there will exist approximately the same generation rate g(d) at any absorption depth:

$$g(d) = d^{-1}{\cdot}\eta_i{\cdot}(1\text{-}R){\cdot}N_{ph}, \quad (1)$$

where η_i is the inner quantum efficiency (for MCT $\eta_i \approx 1$), R is the reflection coefficient ($R \approx 0.34$), and N_{ph} is the number of photons falling down on the active photoconductor area. It follows from Eq. (1) that the responsivity will be inversely proportional to the photoconductor active layer depth. It was experimentally proved for the devices on the base of similar layers [37].The layers with the thicknesses *d*, that are thinner than the typical thickness of $d \sim 10$ μm for photoconductors, could be taken down to the 1 μm depth, and the photocurrent generation rate will be almost independent from the layer thicknesses. In fact, for this limit, the photoresponse will depend on the non-equilibrium charge- carrier recombination at the sample surface

$$K = K_0{\cdot}[1 + (2s\tau/d)]^{-1}, \quad (2)$$

where s is the surface recombination rate and τ is the recombination time. The MCT layers, that were used for manufacturing the detectors, have specially designed composition profiles with the wide-band layers at the boundaries (Fig. 5), and that creates the built-in electric field and blocks the surface recombination.

Because of the high photon flux value $N_{ph} \sim 10^{19}$ cm^{-2} s^{-1} from the globar ($T_{globar} \approx 1600$ °C), in the 5.0–5.5 μm spectral range and in the stationary regime of the photoconductivity (modulation frequency f ~ 300 Hz), the photo-induced carriers concentration is $\Delta n = g(d)\cdot\tau \sim 1\cdot10^{15}$ cm^{-3}. For the initial concentration $n_i \sim 2.5\cdot10^{16}$ cm^{-3}, the $\Delta n/n_i$ value is getting $\Delta n/n_i \sim 4\cdot10^{-2}$ and that is quite sufficient to observe the signal-to-noise ratio ~50 (see Fig. 14b) with the lock-in amplifier (Stanford SR 830). The measured recombination time is $\tau \sim 7\cdot10^{-8}$ s in such *n*-type layers. At the background temperature $T_{BLIP} = 300$ K (BLIP – background limited performance) and quantum efficiency $\eta \approx 1$, the uncooled photoconductors can reach the detectivity values $D^* \approx 4\cdot10^8$ cm Hz$^{1/2}$/W at this $\lambda_{cut\text{-}off}$ operating region [38].

5. THz response in HgTe QW structures

The THz photoresponse of QW HgTe structures was mainly considered [see, *e.g.*, 39,40] when placed into the magnetic field at low temperatures.

Despite the interest in the QW response to the THz radiation, to our knowledge, no QW parameters, as detectors, were measured. Here, we investigated the sub-THz photoresponse at T = 80 and 300 K of the gated channel based on the HgTe QW structure, which was presented in [41]. The structure is based on $Hg_{0.7}Cd_{0.3}Te/HgTe/Hg_{0.7}Cd_{0.3}Te$ QWs with the width 6.6 nm, which is close to the critical HgCd QW thickness, has the symmetrical indium-doped barrier layers. The impurity density was rather high, and it was determined as an electron concentration in the QW of around 1.5^*10^{12} cm^{-2}. For the gated channel formation, the QW structure was photo-lithographically processed with a subsequent wet chemical etching into 50 μm wide bars at the distance of 100 and 250 μm between the Ohmic indium contacts. Then a 80 nm thick Al_2O_3 insulator layer was placed by the atomic layer deposition technique. Finally, the Ti/Au gate was deposited.

Here the QW channel of the structure (scheme is shown in Fig. 9) was characterized and tested with the IMPATT diode emitting at a frequency around 140 GHz. The yielded maximum responsivities of S ≈ 0.21 V/W at T 80 K, and S = 0.11 V/W at T = 300 K were obtained when the HgTe QW channel was taken as a bolometer, using source-drain (s-d) contacts with soldered contact wires which served as antennas. The estimated noise equivalent power values were $NEP_{80K} \approx 6\cdot10^{-8}$ W/Hz$^{1/2}$ and $NEP_{300K} \approx 1.5\cdot10^{-7}$ W/Hz$^{1/2}$. These data were obtained at biases $I_{s\text{-}d} = 0$ and $U_g = 0$, where U_g is the gate voltage. The power P at the QW structure with area $l \times W = 250 \times 50$ μm^2 (the effective antenna area was assumed to be $A_{eff} = (\lambda^2/4\pi)\cdot G$, [36], with the antenna gain G = 1) is equal to ≈ 0.4 mW. At source-drain current $I_{s\text{-}d} = \pm 10$ μA responsivity S equals ≈ 1.1 V/W. In Fig. 15 is shown the voltage response dependence on the s-d current. The HgTe QW responsivity can be enlarged with matching the QW and the antenna impedances. However, it is difficult to expect a high QW channel sensitivity, as the relatively short relaxation times [42] do not favor the high HgTe QW detector sensitivity and a poor matching of the QW impedance (≈40 kΩ) and of the antenna (~300 Ω). Moreover, the structure does not show any essential response at the gate voltage change. It is connected with the high doping level: electron gas is strongly degenerated, and the Fermi level is placed high in the conduction band with the Dirac-like spectrum. Therefore, big gate voltage changes do not cause any channel depletion.

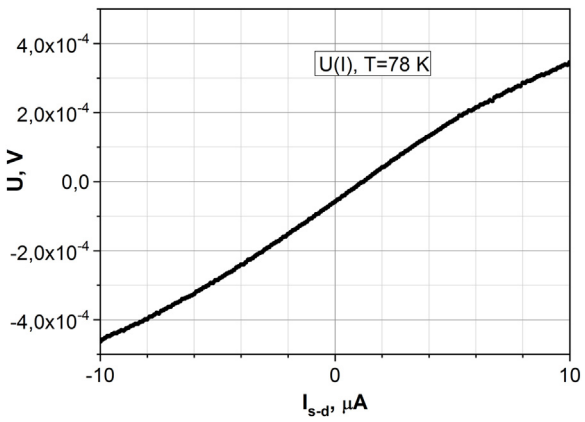

Fig. 15. The QW channel response in the dependence of the current in the channel, $U_g = 0$ V.

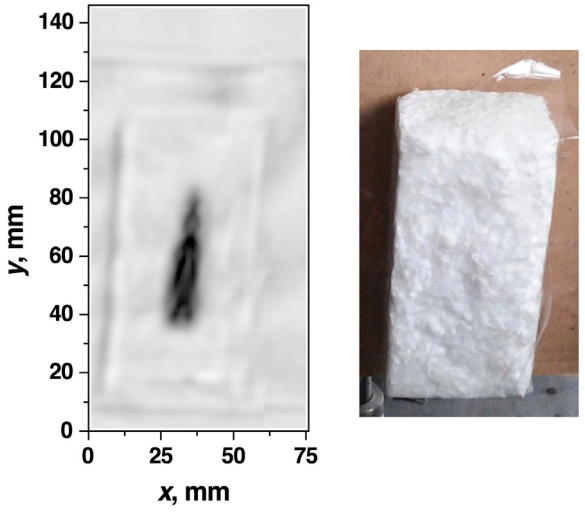

Fig. 16. Bullet hidden in foam plastic packing in non-transparent envelope: left Sub-THz image ($\nu = 143$ GHz); right is the visible image of container.

It was proved that, for the known uncooled detectors, there is no feasibility of passive imaging by direct detection, as NEP does not satisfy the requirements for the passive imaging of the THz system. Our uncooled MCT detector array system can locate and image hidden objects that are either absorbing or reflecting in the THz/sub-THz region and are capable of active imaging. The examples of sub-THz images of the hidden objects obtained by the developed system are shown in Figs. 16 and 17. Traditionally, reflected radiation or radiation passed through an object, which inhomogeneity leads to the formation of a contrast picture, is used in obtaining THz images. To increase the image information capability, our active THz system allows receiving the images of objects in a configuration of transmission and reflection at the same time. The proposed technique allows pointing out metallic parts of objects from others.

6. Conclusions

The developed technology allows the accurate control of molar composition, layer thicknesses and electrical impurity concentrations in the grown structures directly in the growth process. Therefore, the existing technological achievements make it possible to obtain diverse MCT structures with desired parameters.

As an example of the advanced MCT heterostructures growth technology application, we demonstrated an active dual-band

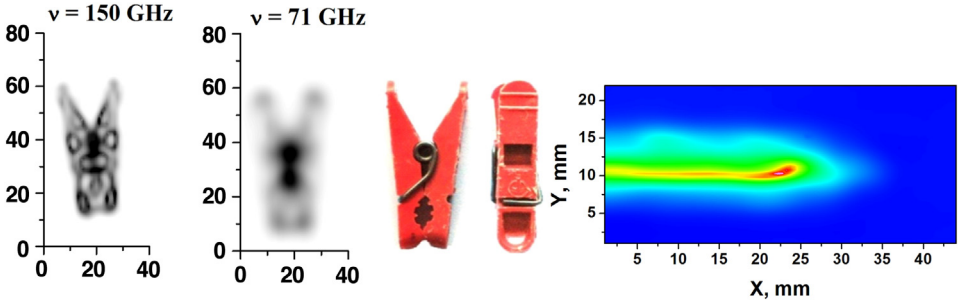

Fig. 17. THz images of the plastic clothes peg in the nontransparent in visible range package: a) logarithmic brightness scale (ν = 150 GHz), b) logarithmic brightness scale (ν = 71 GHz), c) visible picture, (d) Tube ($\varnothing \approx 2.8$ mm) with liquid substance in nontransparent container ($\varnothing \approx 8$ mm), ν = 140 GHz.

detector with a small number of elements in a linear array based on narrow-band HgCdTe bolometric layers, and it is implemented in this project. Their noise equivalent power (NEP) at a frequency $\nu \approx 140$ GHz reached a value of $\sim 2.6\ 10^{-10}$ W/Hz$^{1/2}$ and satisfied the requirements for the active imaging of THz systems. At the same time, these detectors can operate as IR detectors with signal-to-noise ratios S/N of 750 and 50 at T = 78 K and 300 K, respectively. The QW HgTe structures are also encouraging, but can be improved by resolving the problem of matching the QW structures and the antenna impedances and optimizing the carrier concentration and composition.

The THz images of some hidden objects with the dimensions of several millimeters considered here as an imitation of explosive and dangerous substances placed in non-transparent boxes, foam plastic packing and behind the 12 mm thick gypsum board. The THz active optical system with the use of a linear array of uncooled HgCdTe detectors can be implemented for the detection of matters or their shapes, any explosive substances hidden behind non-metallic packagings with dimensions from several mm or larger.

Authors statement

S.A. Dvoretsky – Justification of growth HgCdTe by MBE.

N.N. Mikhailov – Justification of growth HgCdTe and HgTe QW on GaAs by MBE.

V.G. Remesnik – Justification of optical interaction with HgCdTe and HgTe QW and measurements of transmission and reflective spectra for determine the HgCdTe composition *ex-situ*.

Yu.G. Sidorov – Justification of mechanism of growth HgCdTe by MBE, nature and defects formation, thermodynamic calculations.

V.A. Shvets – Justification of ellipsometry and application to measurement HgCdTe composition, growth rate at initial stages and layers thicknesses *in situ*.

D.G. Ikusov – Elaboration of equipment for MBE growth and the providing growth processes of HgCdTe and HgTe QW on GaAs.

V.S. Varavin – Justification of study carries transport in HgCdTe and measuring carrier concertation, mobility and lifetime, Elaboration of equipment and carrying out the thermal annealing processes.

M.V. Yakushev – Justification of growth HgCdTe and HgTe QW on Si by MBE.

J.V. Gumenjuk-Sichevska – Justification of the THz photoresponse at T = 80 and 300 K of the gated channel based HgTe QW structures.

A.G. Golenkov – Elaboration of equipment for THz responsivity measurements and measuring of IR and THz response in HgCdTe and HgTe structures.

I.O. Lysiuk – Measuring of IR and THz responsivity in HgCdTe and HgTe structures, calculations of the results.

Z.F. Tsybrii – Elaboration of antennas and multilayer contacts to HgCdTe and HgTe structures and taking part in measuring of IR and THz responsivity.

A.V. Shevchik-Shekera – Design and manufacture of THz aspherical optics, control of the optical parameters of the THz optics designed.

F.F. Sizov – Justification of the IR and THz sensitivity in intrinsic HgCdTe layers at ambient temperatures.

A.V. Latyshev – academic advising and Justification of transmission electron microscopy of HgCdTe structures.

A.L. Aseev – academic advising and justification of quantum properties of HgTe QW.

Funding

This work was partially supported by grants RBFR "18-52-16007 NTSIL_a", "18-52-16008 NTSIL_a" and 18-29-20053 NTSIL_a the Volkswagen Stiftung Program, and NANO Program.

References

[1] M.A. Kinch, Fundamental physics of infrared detector materials, J. Korean Inst. Electr. Electron. Mater. Eng. 29 (2000) 809–817, http://dx.doi.org/10.1007/s11664-000-0229-7.
[2] M.A. Kinch, HgCdTe: recent trends in the ultimate IR semiconductor, J. Korean Inst. Electr. Electron. Mater. Eng. 39 (2010) 1043–1052, http://dx.doi.org/10.1007/s11664-010-1087-6.
[3] A. Rogalski, Infrared Detectors, second edition, Taylor & Francis Group, 2011.
[4] A. Rogalski, Infrared detectors: an overview, Infrared Phys. Technol. 43 (2002) 187–210, http://dx.doi.org/10.1016/S1350-4495(02)00140-8.
[5] A. Rogalski, J. Antoszewski, L. Faraone, Third-generation infrared photodetector arrays, J. Appl. Phys. 105 (2009) 1–43, http://dx.doi.org/10.1063/1.3099572, 091101.
[6] S.S. Dhillon, M.S. Vitiello, E.H. Linfield, et al., The 2017 terahertz science and technology roadmap, J. Phys. D: App. Phys. 50 (2017) 043001, http://dx.doi.org/10.1088/1361-6463/50/4/043001.
[7] R.A. Lewis, A review of terahertz sources, J. Phys. D: Appl. Phys. 47 (2014) 374001, http://dx.doi.org/10.1088/0022-3727/47/37/374001.
[8] T. Hochrein, Markets, availability, notice, and technical performance of terahertz systems: Historic development, present, and trends, J. Infrared Millim. Terahertz Waves 36 (2015) 235–254.
[9] F. Sizov, THz radiation detectors: state-of-the art, Semicond. Sci. Technol. 33 (2018) 26, http://dx.doi.org/10.1088/1361-6641/aae473, 123001.
[10] E.B. Olshanetsky, S. Sassine, Z.D. Kvon, N.N. Mikhailov, S.A. Dvoretsky, J.C. Portal, A.L. Aseev, Quantum Hall liquid-insulator and plateau-to-plateau transitions in a high mobility 2DEG in a HgTe quantum well, Pis'ma v ZhETF 84 (2006) 661–665, http://dx.doi.org/10.1134/S0021364006220085.
[11] W.D. Lawson, S. Nielson, E.H. Putley, A.S. Young, W.D. Lawson, S. Nielson, E.H. Putley, A.S. Young, Preparation and properties of HgTe and mixed crystals of HgTe-CdTe, J. Phys. Chem. Solids 9 (1959) 325–329, http://dx.doi.org/10.1016/0022-3697(59)90110-6.
[12] Z.D. Kvon, E.B. Olshanetsky, D.A. Kozlov, N.N. Mikhailov, S.A. Dvoretsky, Two-dimensional electron-hole system in a HgTe-based quantum well, JETP Lett. 87 (2008) 502–505, http://dx.doi.org/10.1134/S0021364008090117.
[13] M. König, S. Wiedmann, C. Brüne, A. Roth, H. Buhmann, L.W. Molenkamp, X.-L. Qi, Sh.-Ch. Zhang, Quantum spin hall insulator state in HgTe quantum wells, Science 318 (2007) 766–770, http://dx.doi.org/10.1126/science.1148047.
[14] P. Norton, HgCdTe infrared detectors, Opto-Electron. Rev. 10 (2002) 159–174.
[15] W. Lei, J. Antoszewski, L. Faraone, Progress, challenges, and opportunities for HgCdTe infrared materials and detectors, Appl. Phys. Rev. 2 (2015) 041303, http://dx.doi.org/10.1063/1.3056393.

[16] Yu.G. Sidorov, S.A. Dvoretsky, N.N. Mikhhailov, M.V. Yakushev, V.S. Varavin, A.P. Antsiferov, Molecular-beam epitaxy of narrow-band $Cd_xHg_{1-x}Te$. Equipment and technology, J. Opt. Technol. 67 (2000) 31–36, http://dx.doi.org/10.1364/JOT.67.000031.
[17] K.K. Svitashev, S.A. Dvoretsky, Yu.G. Sidorov, A.S. Mardezhov, I.E. Nis, V.S. Varavin, V.I. Liberman, V.G. Remesnik, The growth of high-quality MCT films by MBE using in-situ ellipsometry, Cryst. Res. Technol. 29 (1994) 931–937, http://dx.doi.org/10.1002/crat.2170290703.
[18] E.V. Spesivtsev, S.V. Rykhlitski, Licence No 16314 Bulletin "Useful Models. Industrial Samples", vol. 35, 2000 (in Russian).
[19] Yu.G. Sidorov, S.A. Dvoretsky, N.N. Mikhailov, M.V. Yakushev, I.V. Sabinina, Molecular beam epitaxy of MCT solid solution on alternative substrate, Semiconductors 35 (2001) 1045, http://dx.doi.org/10.1134/1.1403569.
[20] V.A. Shvets, N.N. Mikhailov, M.V. Yakushev, E.V. Spesivtsev, Ellipsometric measurements of the optical constants of solids under impulse heating, Proc. SPIE 4900 (2002) 46–52, http://dx.doi.org/10.1117/12.484591.
[21] V.A. Shvets, S.V. Rykhlitski, E.V. Spesivtsev, N.A. Aulchenko, N.N. Mikhailov, S.A. Dvoretsky, Yu.G. Sidorov, R.N. Smirnov, In situ ellipsometry for control of $Hg_{1-x}Cd_xTe$ nanolayer structures and ingomogeneous during MBE growth, Thin Solid Films 455–456 (2004) 688–694 http://dspace.nbuv.gov.ua/handle/123456789/118333.
[22] V.S. Varavin, S.A. Dvoretsky, V.I. Liberman, N.N. Mikhailov, Yu.G. Sidorov, Molecular beam epitaxy of high quality Hg_{1-x} Cd_xTe films with control of the composition distribution, J. Cryst. Growth 159 (1996) 1161–1166, http://dx.doi.org/10.1016/0022-0248(95)00845-4.
[23] V.M. Osadchiy, A.O. Suslyakov, V.V. Vasil'ev, S.A. Dvoretsky, The effective minority lifetime in CdHgTe with graded layers grown by MBE, Avtometriya 4 (1998) 71–77 (in Russian).
[24] S.M. Johnson, D.R. Rhiger, J.P. Rosbeck, J.M. Peterson, S.M. Taylor, M.E. Boyd, Effect of dislocations on the electrical and optical properties of long-wavelength infrared HgCdTe photovoltaic detectors, J. Vac. Sci. Technol. B: Microelectron. Nanometer Struct. Process. Meas. Phenom. 10 (1992) 1499–1506, http://dx.doi.org/10.1116/1.586278.
[25] P.A. Bakhtin, S.A. Dvoretskii, V.S. Varavin, A.P. Korobkin, N.N. Mikhailov, I.V. Sabinina, Yu.G. Sidorov, Effect of low-temperature annealing on electrical properties of n-HgCdTe, Semiconductors 38 (2004) 1172, http://dx.doi.org/10.1134/1.1808823.
[26] S. Dvoretsky, N. Mikhailov, Yu. Sidorov, V. Shvets, S. Danilov, B. Wittman, S. Ganichev, Growth of HgTe quantum wells for IR to THz detectors, J. Electron. Mater. 39 (2010) 918–923, http://dx.doi.org/10.1007/s11664-010-1191-7.
[27] H. Arwin, D.E. Aspnes, Nondestructive analysis of $Hg_{1-x}Cd_xTe$ (x=0.00, 0.20, 0.29, and 1.00) by spectroscopic ellipsometry. II. Substrate, oxide, and interface properties, J. Vac. Sci. Technol. A 2 (1984) 1316, http://dx.doi.org/10.1116/1.572401.
[28] L. Vina, C. Umbach, M. Cardona, L. Vodopjanov, Ellipsometric studies of electronic interband transitions in CdxHg1-xTe, Phys. Rev. B 29 (1984) 6752–6760, http://dx.doi.org/10.1103/PhysRevB.29.6752.
[29] F. Sizov, Z. Tsybrii, V. Zabudsky, M. Sakhno, A. Shevchik-Shekera, M. Smoliy, E. Dieguez, S. Dvoretsky, Possibility of the detection in IR and sub/THz spectral region using MCT thin layer receivers: design of the chip, optical elements and antenna pattern, IEEE MMS 2015 (2015) 49–52, http://dx.doi.org/10.1109/MMS.2015.7375429.
[30] F. Sizov, Z. Tsybrii, V. Zabudsky, O. Golenkov, V. Petryiakov, S. Dvoretsky, N. Michailov, A. Shevchik-Shekera, I. Lysiuk, E. Dieguez, Mercury–cadmium–telluride thin layers as sub-terahertz and infrared detectors, Opt. Eng. 54 (2015) 12127102, http://dx.doi.org/10.1117/1.OE.54.12.127102.
[31] V. Dobrovolski, F. Sizov, THz/sub-THz bolometer based on electron heating in a semiconductor waveguide, Optoelectr. Rev. 18 (2010) 250–258, http://dx.doi.org/10.2478/s11772-010-1033-8.
[32] M.A. Kinch, B.V. Rollin, Detection of millimetre and sub−millimetre wave radiation by free carrier absorption in a semiconductor, Brit. J. Appl. Phys. 14 (1963) 672–676, http://dx.doi.org/10.1088/0508-3443/14/10/317.
[33] V. Zabudsky, F. Sizov, N. Momot, Z. Tsybrii, N. Sakhno, S. Bunchuk, N. Michailov, V. Varavin, THz/sub-THz direct detection detector on the base of electrons/holes heating in MCT layers, Semicond. Sci. Technol. 27 (2012) 045002, http://dx.doi.org/10.1088/0268-1242/27/4/045002.
[34] M. Sakhno, A. Golenkov, F. Sizov, Uncooled detector challenges: millimeter-wave and terahertz long channel field effect transistor and Schottky barrier diode detectors, J. Appl. Phys. 114 (2013) 164503, http://dx.doi.org/10.1063/1.4826364.
[35] F. Sizov, V. Zabudsky, S. Dvoretskii, V. Petryakov, O. Golenkov, K. Andreyeva, Z. Tsybrii, Two-colour detector: mercury-cadmium-telluride as a terahertz and infrared detector, Appl. Phys. Lett. 106 (2015) 082104, http://dx.doi.org/10.1063/1.4913590.
[36] A.C. Balanis, Antenna Theory: Analysis and Design, 3rd ed., J. Wiley & Sons, Inc., New York, 2005.
[37] G. Chekanova, M. Nikitin, S. Lartsev, V. Varavin, N. Michailov, Photoresistive infrared detectors on the base of CdHgTe/CdTe/ZnTe/GaAs heterostructures, in: A. Aseev (Ed.), Photoreceivers on the Base of Mercury-Cadmium-Telluride Epitaxial System, 2012, 202–207, Novosibirsk, Russia (in Russian).
[38] J. Piotrowski, A. Rogalski, Uncooled long wavelength infrared photon detectors, Infr. Phys. Technol. 46 (2004) 115–131, http://dx.doi.org/10.1016/j.infrared.2004.03.016.
[39] F. Gouider, M. Bugár, J. Könemann, Yu.B. Vasilyev, C. Brüne, H. Buhmann, G. Nachtwei, THz photoresponse and magnetotransport of detectors made of HgCdTe/HgTe quantum well structures, J. Phys.: Conf. Ser. 193 (2009) 012066, http://dx.doi.org/10.1088/1742-6596/193/1/012066.
[40] A.M. Kadykov, C. Consejo, M. Marcinkiewicz, L. Viti, M.S. Vitiello, S.S. Krishtopenko, S. Ruffenach, S.V. Morozov, W. Desrat, N. Dyakonova, W. Knap, V.I. Gavrilenko, N.N. Mikhailov, S.A. Dvoretsky, F. Teppe, Observation of topological phase transition by terahertz photoconductivity in HgTe-based transistors, Phys. Status Solidi C 13 (2016) 534–537, http://dx.doi.org/10.1063/1.4932943.
[41] D.A. Kozlov, Z.D. Kvon, N.N. Mikhailov, S.A. Dvoretskii, S. Weishäupl, Y. Krupko, J.-C. Portal, Quantum hall effect in HgTe quantum wells at nitrogen temperatures, Appl. Phys. Lett. 105 (2014) 132102, http://dx.doi.org/10.1063/1.4896682.
[42] S.N. Danilov, B. Wittmann, P. Olbrich, W. Eder, W. Prettl, L.E. Golub, E.V. Beregulin, Z.D. Kvon, N.N. Mikhailov, S.A. Dvoretsky, V.A. Shalygin, N.Q. Vinh, A.F.G. van der Meer, B. Murdin, S.D. Ganichev, J. Appl. Phys. 105 (2009) 013106, http://dx.doi.org/10.1063/1.3056393.